PHYSICAL REVIEW LETTERS

Optimized Double-Well Quantum Interferometry with Gaussian Squeezed States

Y. P. Huang and M. G. Moore

Department of Physics and Astronomy, Michigan State University, East Lansing, Michigan 48824, USA

A Mach-Zender interferometer with a Gaussian number-difference squeezed input state can exhibit sub-shot-noise phase resolution over a large phase interval. We derive the optimal level of squeezing for a given phase interval $\Delta\theta_0$ and particle number N. We then propose an adaptive measurement sequence in which the amount of squeezing is increased with each measurement. With this scheme, any phase on $(-\Delta\theta_0, \Delta\theta_0)$ can be measured with a precision of $3.5/N$, requiring only 2–4 measurements, provided only that $N\tan(\Delta\theta_0) < 10^{40}$. In a double-well Bose-Einstein condensate, the optimized input states can be created by adiabatic manipulation of the ground state.

Measuring an arbitrary phase with precision well above the standard quantum limit (SQL) has been a long-standing challenge in quantum interferometry [1–4]. The SQL minimum phase uncertainty is $1/\sqrt{N_{\text{tot}}}$, but the theoretical lower limit to the phase uncertainty, known as the Heisenberg limit (HL), is $1/N_{\text{tot}}$, where N_{tot} is the total number of particles used in the determination of the phase. There have been many proposals to achieve $1/N_{\text{tot}}$ scaling in a two-input interferometer, using number-difference squeezed input states [1–3,5], coherent and/or squeezed-vacuum input states [6–8], or the maximally entangled N-particle NOON state $\frac{1}{2}(|N, 0\rangle + |0, N\rangle)$ [9–12]. Recently, the double-well Bose-Einstein condensate (BEC) has emerged as a promising system for high-precision matter-wave interferometry [13–17], including progress towards atom counting at the single-particle level [18,19]. For this system, the squeezed-vacuum protocols are not applicable, and the NOON state is highly problematic due to the periodicity of the phase distribution [20,21], leaving the number-difference squeezed state as the most viable candidate. With such squeezed states, however, there has yet been no systematic study of how to measure an arbitrary nonzero phase at or near HL precision in the large-N limit. In this Letter, we perform such an analysis and show that an asymptotic scaling of $[\ln(\ln N_{\text{tot}})]/N_{\text{tot}}$ can be achieved via multiple adaptive measurements with Gaussian number-squeezed states, which can be readily created in a double-well BEC.

For measuring a phase of $\theta = 0$, it has been shown that the Twin-Fock (TF) state and the related Pezze-Smerzi (PS) state can achieve Heisenberg scaling [20,22–24]. We find, however, for $\theta \neq 0$ that the phase uncertainty of the TF and PS states rapidly decay to worse than the SQL and, in the limit of large N, approach constant values, independent of N. While the PS state was investigated only for $\theta = 0$, Kim *et al.* [24] investigated $\theta \neq 0$ for the TF state with $N = 100$. They observe a phase uncertainty $\sim 1/N_{\text{tot}}$ for $\theta < 1/N$ and growing rapidly thereafter. Our results similarly indicate that the TF and PS states become worse than the shot noise for $\theta \gg 1/N$.

To find the optimal input state, we constrain ourselves to the ground states of a double-well BEC with repulsive interactions for experimental obtainability. The double-well BEC system is described by the Hamiltonian

$$\hat{H}(\chi) = -2\tau\hat{J}_x + \delta\hat{J}_z + U\hat{J}_z^2, \qquad (1)$$

where τ is the interwell tunneling rate, U is the atom-atom interaction strength, and δ is the asymmetric tilt of the double well, presumably due to the external perturbation being measured. The angular momentum operators are defined as $\hat{J}_x = \frac{1}{2}(\hat{c}_L^\dagger\hat{c}_R + \hat{c}_R^\dagger\hat{c}_L)$, $\hat{J}_y = \frac{1}{2i}(\hat{c}_L^\dagger\hat{c}_R - \hat{c}_R^\dagger\hat{c}_L)$, and $\hat{J}_z = \frac{1}{2}(\hat{c}_L^\dagger\hat{c}_L - \hat{c}_R^\dagger\hat{c}_R)$, with $\hat{c}_L$ and $\hat{c}_R$ being the annihilation operators for particles in the two localized modes. For repulsive atom-atom interaction and $\delta \approx 0$, the ground state is very close to a Gaussian squeezed (GS) state of the form $|\sigma\rangle \propto \sum_{n=-N/2}^{N/2} e^{-n^2/4\sigma^2}|n\rangle$, where $|n\rangle$ is a number-difference eigenstate satisfying $\hat{J}_z|n\rangle = n|n\rangle$. The width σ depends on the parameter $u = U/\tau$ and is given by $\sigma^2 = N/4\sqrt{1 + uN}$ [25]. The squeezing parameter for the state is then $s = 2\sigma/\sqrt{N}$. The nature of our adaptive measurement scheme requires that we tune u to an optimal value which takes into account our prior knowledge of N and θ; thus, we have $u \rightarrow u(N, \theta)$. This tuning is accomplished by varying U/τ via a Feshbach resonance and/or changing the shape of the double-well potential and allows σ to be varied between 0 and $\sqrt{N}/2$, corresponding to maximal number-difference squeezing and no squeezing, respectively.

To implement a Mach-Zehnder interferometer (MZI), we set $U = 0$ and allow tunneling for $t = \pi/4\tau$ duration, thus realizing a linear 50/50 beam splitter, described by the propagator $e^{i(\pi/2)\hat{J}_x}$. This is followed by a sudden raising of the potential barrier to turn off tunneling and allow phase acquisition due to the small but nonvanishing δ. By holding the system for a measurement time T, a phase shift of $\theta = -\delta T$ will be acquired, described by the propagator $e^{i\theta\hat{J}_z}$. The barrier is then lowered again to implement a second beam splitter.

In the MZI, a symmetric input state $|\Psi_{in}\rangle$ is transformed into the phase-dependent output state $|\Psi_{out}\rangle = e^{i(\pi/2)\hat{J}_x}e^{i\theta\hat{J}_z}e^{i(\pi/2)\hat{J}_x}|\Psi_{in}\rangle = e^{-i\theta\hat{J}_y}e^{i\pi\hat{J}_x}|\Psi_{in}\rangle$ [1]. Applying this transformation to a typical GS state results in an output state whose properties are easily understood using the Bloch-sphere quasiprobability distribution [5], which assigns a probability to each point on a sphere of radius $N/2$ according to $P(\theta, \phi) = |\langle N/2|e^{i\hat{J}_y(\pi/2-\theta)}e^{i\hat{J}_z\phi}|\Psi_{out}\rangle|^2$. In this picture, the TF and PS states are thin equatorial rings, and a GS input state is an ellipse centered on the J_x axis, compressed along the J_z direction. Typical GS input and output states are shown in Fig. 1(a).

Phase information is obtained by measuring the number difference between the two interferometer modes, which projects the output state onto a $\hat{J}_z$ eigenstate. Quantum fluctuations in this measurement are governed by the projection of the output distribution onto the J_z axis. Because of the rigid rotation, the width of the projection will be determined by a θ-dependent combination of the J_z and J_x noise of the input distribution. The goal of this Letter is thus to find the optimal amount of squeezing to minimize the phase uncertainty given a fixed particle number N and an initial estimated phase θ_0 with uncertainty $\Delta\theta_0$.

Before we present numerical results from a rigorous Bayesian analysis, we first use linearized error propagation to provide an approximate analytical description of the interferometer performance. An analytical result is important for predicting the behavior at large N, where a nu-
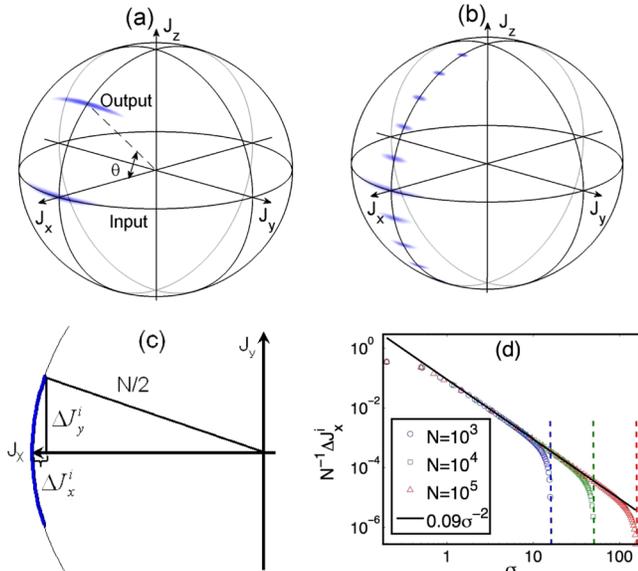

FIG. 1 (color online).   Bloch-sphere analysis of the MZI with a GS input state: (a) A typical GS state at input and output stages; (b) output states for optimized input states with $\theta = 0$, $\pm\frac{\pi}{12}$, $\pm\frac{\pi}{6}$, $\pm\frac{\pi}{4}$, $\pm\frac{\pi}{3}$, $\pm\frac{5\pi}{12}$; (c) geometric origin of the J_x input noise ΔJ_x^i; (d) numerical results plotting $\Delta J_x^i/N$ versus σ on a log-log scale for three different N values, validating the functional form of ΔJ_x^i derived geometrically from (c). The dashed vertical lines correspond to $\sigma = \frac{\sqrt{N}}{2}$, where ΔJ_x^i drops to zero.

merical result is inaccessible. In this approach, the phase uncertainty is estimated by evaluating $\Delta\theta = [\partial\langle\hat{J}_z\rangle/\partial\theta]^{-1}\Delta J_z$ at the interferometer output. For input states symmetric around $n = 0$, the expectation values at the output are related to those at the input via $\langle\hat{J}_z\rangle = \sin\theta\langle\hat{J}_x^i\rangle$ and $\Delta J_z = \sqrt{\cos^2\theta\Delta J_z^{i2} + \sin^2\theta\Delta J_x^{i2}}$. For GS states, $\langle\hat{J}_x^i\rangle \approx N/2$ and $\Delta J_z^i = \sigma$, which immediately leads to $\langle\hat{J}_z\rangle = N(\sin\theta)/2$. In Fig. 1(c), we see that $\Delta J_x^i \approx N/2 - \sqrt{N^2/4 - \Delta J_y^{i2}}$. Since the GS state is a minimum uncertainty state with $\Delta J_y^i\Delta J_z^i = \langle\hat{J}_x^i\rangle/2$, we see that $\Delta J_y^i = N/4\sigma$. This leads to $\Delta J_x^i = \alpha N/\sigma^2$, with $\alpha \approx 0.06$. Exact numerical calculations verify this analytic form for $1 \ll \sigma \ll \sqrt{N}/2$, as shown in Fig. 1(d), but with $\alpha = 0.09$. By inserting these results into the error-propagation formula, we find

$$\Delta\theta \approx \frac{2\sigma}{N}\sqrt{1 + \left[\frac{0.09N\tan\theta}{\sigma^3}\right]^2}. \qquad (2)$$

The TF and PS states roughly correspond to a fixed $\sigma \lesssim 1$, resulting in $\lim_{N\to\infty}\Delta\theta = 0.18\tan\theta/\sigma^2$, which quickly becomes saturated to an N-independent constant for $\theta \gg 1/N$, a result we have verified numerically with exact Bayesian calculations. On the other hand, if holding u fixed so that $\sigma \sim N^{1/4}$, the phase uncertainty scales as $\Delta\theta \sim 1/N^{3/4}$ for $\theta = 0$, as discussed in Ref. [26], and would eventually saturate to $\sim 1/\sqrt{N}$ for $\theta \neq 0$. Rather than holding σ or u fixed, we propose varying u and thus σ with N in order to minimize the phase variance. By setting $d\Delta\theta/d\sigma = 0$, we find

$$\sigma_{min}(\theta, N) \approx 0.503(N\tan|\theta|)^{1/3}, \qquad (3)$$

$$\Delta\theta_{min}(\theta, N) \approx 1.23(\tan|\theta|)^{1/3}/N^{2/3}. \qquad (4)$$

From self-consistency, these expressions are valid only when $10/N \lesssim |\theta| \lesssim \tan^{-1}(0.137\sqrt{N}) \approx \pi/2$.

We now employ rigorous Bayesian analysis to quantify the phase uncertainty and validate our approximate analytic results, again assuming that $|\theta|$ is not too close to $\pi/2$. According to the Bayes theorem, upon a measurement result n_m, the probability that the actual phase is ϕ is $P(\phi|n_m) = P(n_m|\phi)/\int d\theta P(n_m|\theta)$, where $P(n|\theta) = |\langle n|e^{-i\theta\hat{J}_y}|\psi_{in}\rangle|^2$. The error-propagation result (4) is very close to the 68% confidence interval of $P(\phi|n)$ because the underlying number distribution of the optimized GS output state is well approximated by a Gaussian distribution $P(n|\theta) \approx [\sqrt{2\pi}\Delta n]^{-1}e^{-(n-N\sin\theta/2)^2/2\Delta n^2}$. This shows that the most-probable outcome is $\bar{n} = N\sin\theta/2$, which is sensitive to the sign of θ. Because Δn is only weakly dependent on θ, the inverted distribution $P(\phi|n)$ will also be close to Gaussian in the small-angle regime, with a width given by (4). To make a theoretical performance analysis for a fixed θ, we average over all possible mea-

surement outcomes, defining $P(\phi|\theta) = \sum_n P(\phi|n)P(n|\theta)$ [22,23]. This can be interpreted as the probability for an experimenter to infer ϕ given a true phase shift of θ. The phase uncertainty $\Delta\theta$ is then defined as the 68% confidence interval, via $\int_{\theta-\Delta\theta}^{\theta+\Delta\theta} d\phi P(\phi|\theta) = 0.68$.

By using this approach, together with the exact double-well ground state, we numerically find u_{min}, the value of U/τ which minimizes the phase uncertainty. In Fig. 2(a), we plot the corresponding $\sigma_{min} = \sigma(u_{min})$ as a function of N for several θs. Also shown is a least-squares fit to the $N > 10^3$ data (including many data points not shown explicitly) to the analytic form (3), giving

$$\sigma_{min}(\theta, N) = \begin{cases} 1.00, & |\theta| < 10/N, \\ 0.45(N\tan|\theta|)^{1/3}, & |\theta| > 10/N, \end{cases} \quad (5)$$

in good agreement with our analytical result. By inverting Eq. (5) this leads to

$$u_{min}(\theta, N) = \begin{cases} \frac{N}{16} - \frac{1}{N}, & |\theta| < 10/N, \\ \frac{1.52}{(\tan|\theta|)^{4/3}N^{1/3}} - \frac{1}{N}, & |\theta| > 10/N. \end{cases} \quad (6)$$

In Fig. 2(b), we plot the corresponding minimized $\Delta\theta_{min}$ versus N for several phases, achieved by setting $\sigma = \sigma_{min}(\theta, N)$. Again fitting the $N > 10^3$ data to the analytic form of (4), we find

$$\Delta\theta_{min}(\theta, N) = \begin{cases} 3.50/N, & |\theta| < 10/N, \\ 1.63(\tan|\theta|)^{1/3}/N^{2/3}, & |\theta| > 10/N. \end{cases} \quad (7)$$
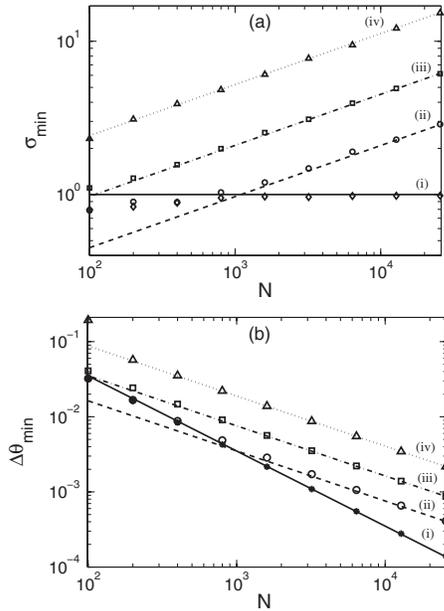

FIG. 2.   (a) Optimal width σ_{min} versus N for different θ; (b) corresponding minimized phase uncertainty $\Delta\theta_{min}$. In both figures, from (i) to (iv) the interferometer phases are $\theta = 0, 0.01, 0.1$, and 1, respectively. The data points represent numerical results from strict Bayesian analysis using the exact ground states of a double-well BEC, while the straight lines represent the asymptotical forms of Eqs. (5) and (7), respectively.

The difference between the prefactor here and (4) is primarily due to a factor of approximately $\sqrt{2}$ which comes from the definition of $P(\phi|\theta)$.

In practice, θ is not known *a priori*; hence, it is not clear what value for θ to use in determining $\sigma_{min}(\theta, N)$ via Eq. (5). If we assume prior knowledge of the form $P(\theta) \propto \exp[-(\theta - \theta_0)^2/2\Delta\theta_0^2]$, we should first remove θ_0 by adding θ_0/T to the tilt δ during phase acquisition and then use $\sigma_{min}(\Delta\theta_0, N)$. After obtaining a measurement result n_1, the estimated uncertainty $\Delta\theta_1$ is then determined via $\int_{\theta_1-\Delta\theta_1}^{\theta_1+\Delta\theta_1} d\theta' P(\theta'|n_1)$, with $P(\theta'|n_1)$ being given by the Bayes theorem. This will result in $\Delta\theta_1 \sim \Delta\theta_{min}(\Delta\theta_0, N)$. Based on Eq. (7), this uncertainty appears to scale only as $N^{-2/3}$, only a slight improvement of $N^{1/6}$ over the SQL. However, in many applications requiring high precision, the phases are very small, in which case the phase uncertainty can be reduced considerably due to the explicit phase dependence in (7). This is in contrast to a shot-noise-limited interferometer, where $\Delta\theta = 1/\sqrt{N}$ for any θ not too close to $\pm\pi/2$. The explicit θ dependence in the optimized scheme is due to the fact that stronger number squeezing can be tolerated at smaller angles before the $\hat{J}_x^i$ noise becomes detrimental. For example, if the phase is known to be smaller than $1/\sqrt{N}$, we have $\Delta\theta_{min} \lesssim 1.63/N^{5/6}$, which is now an $N^{1/3}$ improvement over the SQL. As can be seen from Eq. (7), a maximum sensitivity of $3.5/N$ can be achieved for $|\theta| < 10/N$, which is true Heisenberg scaling.

In fact, almost any phase between $-\pi/2$ and $\pi/2$ can be measured at the maximum precision of $3.5/N$ if the present scheme is combined with multiple adaptive measurements [1,7]. After the first measurement as described above, we can again rebalance the interferometer by adding θ_1/T to the tilt [27], followed by a second measurement with $\sigma_2 = \sigma_{min}(\Delta\theta_1, N)$, with result n_2. The Bayesian distribution for θ_2 will then be approximately $P(\theta_2|n_2, n_1) \propto \exp[-(\theta_2 - \bar{\theta}_2)^2/2y_2^2]$, where $\bar{\theta}_j = \sin^{-1}(2n_j/N)$ and $1/y_j^2 = \sum_{k=0}^j 1/\Delta\theta_k^2$. Since $\Delta\theta_j$ is much smaller than $\Delta\theta_{j-1}$, we can say $y_j \approx \Delta\theta_j \sim \Delta\theta_{min}(\Delta\theta_{j-1}, N)$. In other words, since the distribution after a measurement is much narrower than the previous distribution, multiplying the distributions has little effect, so that the final uncertainty is effectively determined by the resolution of the final measurement alone. After M iterations, with $\sigma_j = \sigma_{min}(\Delta\theta_{j-1}, N) \approx 0.57(N\tan\Delta\theta_0/2.1)^{3^{-j}}$, we find $\Delta\theta_M \sim (2.1/N)(N\tan\Delta\theta_0/2.1)^{3^{-M}}$. While these expressions are good estimates of the expected behavior, in practice each σ_j and $\Delta\theta_j$ would be computed exactly by applying the Bayes theorem after each measurement. This procedure should be repeated only until $\Delta\theta_M \lesssim 10/N$, after which an addition measurement will push the phase uncertainty to $3.5/N$. The final measurement is then made using the GS state with $\sigma = 1$, which lies at the edge of the maximally squeezed Fock regime defined by $\sigma \ll 1$. Thus an arbitrary phase can be measured at $3.5/N$ precision with $M + 1$

measurements in total. Setting $\Delta\theta_M = 10/N$ and solving for M gives

$$M \approx 0.9\ln[\ln(N\tan\Delta\theta_0/2.1)] - 0.4, \qquad (8)$$

where again this is just an estimate subject to run-to-run fluctuations. For $\theta_r = \pi/3$ and $N = 10^4$, $M = 1.6$, i.e., <3 total measurements will be required. For $N = 10^{12}$, $M = 2.6$, requiring <4 measurements. In fact, the estimated total measurement number will be ≤ 4, provided only that $N\tan(\Delta\theta_0) < 10^{40}$, which corresponds to a phase window of $\Delta\theta_0 = \pi/2 - N/10^{40} \approx \pi/2$.

The final experimental value for the initial unknown phase is then $\theta = \sum_{j=1}^{M+1} \theta_j$ with uncertainty $\Delta\theta = 3.5/N$. The total number of atoms used to obtain this precision is $N_{\text{tot}} = (M + 1)N$. For large enough N, we can approximate $\ln[N_{\text{tot}}/2(M + 1)] \approx \ln(N_{\text{tot}})$, so that $M + 1 \approx 0.9\ln[\ln(N_{\text{tot}}\tan\Delta\theta_0)] + 0.6$, which leads to the asymptotic scaling law

$$\Delta\theta \approx \{2.1 + 3.2\ln[\ln(N_{\text{tot}}\tan\Delta\theta_0)]\}/N_{\text{tot}}. \qquad (9)$$

That the scaling law should depend on the initial phase interval has been previously pointed out [28]. For a typical value of $M \sim 3$, the final phase uncertainty will thus be $\Delta\theta \sim 10/N_{\text{tot}}$.

In order to verify the accuracy of Eq. (8), we carried out exact Monte Carlo simulations of many measurements of the phase $\pi/6$, with an initial uncertainty $\Delta\theta_0 = \pi/3$. During each simulation run, the measurement outcome was randomly selected according to the output distribution, and the phase information was determined numerically via the Bayes theorem. The prescribed measure-rebalance process was iterated until the estimated phase uncertainty reached $3.5/N$. We obtained average values of $\overline{M + 1} = 2.2$ for $N = 500$, and 2.5 for 5000, which agree with Eq. (8). The observed variances $\Delta(M + 1)$ were 0.4 and 0.6, respectively.

For TF and PS states, similar adaptive measurement schemes are extremely inefficient. While their inability to distinguish positive from negative phases makes rebalancing difficult, the primary difficulty is that the phase uncertainty is N-independent for large phases, so that $\sim N^2$ measurements are required to obtain $1/N$ precision. This results in $1/N_{\text{tot}}^{1/3}$ scaling, worse than SQL.

The above discussions have assumed that the input state is optimally squeezed to width $\sigma_{\min}$. A realistic input state, however, may deviate from $\sigma_{\min}$, due to imprecise control over u and/or imprecise knowledge of N. A straightforward error analysis shows that our scheme is extremely robust against such uncertainties. The relative increase in the single-measurement phase uncertainty $\delta\Delta\theta$ due to fluctuations in u and N is found to be $\delta\Delta\theta/\Delta\theta_{\min} = (2/3)\delta N/N + (1/8)(\delta u/u_{\min})^2$. The scaling with δu^2 reflects the fact that $u = u_{\min}$ is a local minimum with respect to the phase uncertainty. Thus a 10% variation in N results in a 7% variation in the phase uncertainty, while

even a 100% uncertainty in u results only in a 13% variation. For our purposes, these increases are essentially negligible and are independent of the values of N or θ. Of course, there are many other potential sources of error, e.g., the precision with which the tilt can be rebalanced and the precision with which the scattering length can be set to zero during interferometer operation. Reaching the Heisenberg limit in a double-well BEC interferometer will clearly require major technological advances in many areas. Assuming that a level of precision significantly below the SQL is eventually obtained, the scheme we have developed will be the optimal method to obtain this precision, whether or not it is close to the Heisenberg limit.

[1] B. Yurke, S. L. McCall, and J. R. Klauder, Phys. Rev. A **33**, 4033 (1986).
[2] M. J. Holland and K. Burnett, Phys. Rev. Lett. **71**, 1355 (1993).
[3] P. Bouyer and M. A. Kasevich, Phys. Rev. A **56**, R1083 (1997).
[4] V. Giovannetti, S. Lloyd, and L. Maccone, Science **306**, 1330 (2004).
[5] K. Eckert *et al.*, Phys. Rev. A **73**, 013814 (2006).
[6] C. M. Caves, Phys. Rev. D **23**, 1693 (1981).
[7] D. Denot, T. Bschorr, and M. Freyberger, Phys. Rev. A **73**, 013824 (2006).
[8] L. Pezzé and A. Smerzi, Phys. Rev. Lett. **100**, 073601 (2008).
[9] J. J. Bollinger, W. M. Itano, D. J. Wineland, and D. J. Heinzen, Phys. Rev. A **54**, R4649 (1996).
[10] C. C. Gerry, Phys. Rev. A **61**, 043811 (2000).
[11] W. J. Munro, K. Nemoto, G. J. Milburn, and S. L. Braunstein, Phys. Rev. A **66**, 023819 (2002).
[12] S. F. Huelga *et al.*, Phys. Rev. Lett. **79**, 3865 (1997).
[13] T. Schumm *et al.*, Nature Phys. **1**, 57 (2005).
[14] R. Gati *et al.*, Appl. Phys. B **82**, 207 (2006).
[15] G.-B. Jo *et al.*, Phys. Rev. Lett. **98**, 030407 (2007).
[16] C. Lee, Phys. Rev. Lett. **97**, 150402 (2006).
[17] L. Pezzé *et al.*, Phys. Rev. A **74**, 033610 (2006).
[18] C.-S. Chuu *et al.*, Phys. Rev. Lett. **95**, 260403 (2005).
[19] M. Shellekens *et al.*, Science **310**, 648 (2005).
[20] Z. Hradil and J. Řeháček, Phys. Lett. A **334**, 267 (2005).
[21] L. Pezzé and A. Smerzi, arXiv:quant-ph/0508158.
[22] L. Pezzé and A. Smerzi, Phys. Rev. A **73**, 011801(R) (2006).
[23] H. Uys and P. Meystre, Phys. Rev. A **76**, 013804 (2007).
[24] T. Kim *et al.*, Phys. Rev. A **57**, 4004 (1998).
[25] A. Imamoğlu, M. Lewenstein, and L. You, Phys. Rev. Lett. **78**, 2511 (1997).
[26] L. Pezzé *et al.*, Phys. Rev. A **72**, 043612 (2005).
[27] D. R. Dounas-Frazer, A. M. Hermundstad, and L. D. Carr, Phys. Rev. Lett. **99**, 200402 (2007).
[28] G. A. Durkin and J. P. Dowling, Phys. Rev. Lett. **99**, 070801 (2007).